

Carbon Nanotube Schottky Diodes Using Ti–Schottky and Pt–Ohmic Contacts for High Frequency Applications

Harish M. Manohara,* Eric W. Wong, Erich Schlecht, Brian D. Hunt, and Peter H. Siegel

Jet Propulsion Laboratory, California Institute of Technology, 4800 Oak Grove Drive, Pasadena, California 91109

Received May 4, 2005; Revised Manuscript Received May 13, 2005

ABSTRACT

We have demonstrated Schottky diodes using semiconducting single-walled nanotubes (s-SWNTs) with titanium Schottky and platinum Ohmic contacts for high-frequency applications. The diodes are fabricated using angled evaporation of dissimilar metal contacts over an s-SWNT. The devices demonstrate rectifying behavior with large reverse bias breakdown voltages of greater than -15 V. To decrease the series resistance, multiple SWNTs are grown in parallel in a single device, and the metallic tubes are burnt-out selectively. At low biases these diodes showed ideality factors in the range of 1.5 to 1.9. Modeling of these diodes as direct detectors at room temperature at 2.5 terahertz (THz) frequency indicates noise equivalent powers (NEP) potentially comparable to that of the state-of-the-art gallium arsenide solid-state Schottky diodes, in the range of 10^{-13} W/ $\sqrt{\text{Hz}}$.

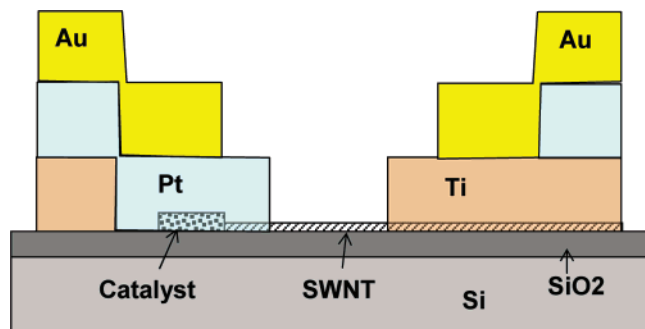
For high-frequency applications in the range of 30 GHz to 3 THz (microwave to submillimeter wave regime), diodes are of particular interest as detectors, mixers, and frequency multipliers.¹ In particular, solid-state Schottky diodes (rectifying metal-semiconductor junctions) are employed because of their higher switching speeds, and their inherent suitability for low-voltage, high-current applications. The state-of-the-art utilizes solid-state Schottky diode detectors for room temperature sensor systems and Schottky diode multipliers for submillimeter wave power generation. However, above a few hundred GHz the inherent parasitic capacitance (proportional to semiconductor junction area) and resistance (inversely proportional to electron mobility) of these devices, because of the limitations of the fabrication process and the material properties, severely limits the achievable sensitivity for detection (direct detector noise equivalent power or NEP $\sim 10^{-12}$ W/ $\sqrt{\text{Hz}}$, heterodyne NEP $\sim 10^{-17}$ W/ $\sqrt{\text{Hz}}$ for cooled operation at 4 K),¹ and generated power at THz frequencies (only microwatts of power up to 1.5 THz).¹ From the material point of view, carbon nanotubes² offer an excellent alternative to their solid-state counterparts because of their small junction areas due to their physical dimensions (< 1 to 2 nm diameter), high electron mobilities (up to 200 000 $\text{cm}^2/\text{V}\text{-s}$ as reported by Durkop et al.),³ and low estimated capacitances (tens of aF/ μm),^{4,5} leading to predicted cutoff frequencies in the THz range.⁵

The electronic properties of single-walled carbon nanotubes (SWNTs) have been studied in detail.^{6–10} The synthesis of SWNTs results in tubes that are either metallic (m-SWNTs) or semiconducting (s-SWNTs) depending on their chirality. Semiconducting SWNTs typically exhibit p-type conductivity for measurements done in air, for reasons still under discussion.^{11–15} Earlier studies have employed s-SWNTs to develop Schottky-barrier-contact field effect transistors (FETs),^{4,16} and rectifying junctions based on CNT defects,⁴ double gates,¹⁷ or crossed m- and s-SWNTs.¹⁸ Burke et al. have studied in detail the AC response of s-SWNT-FETs using phenomenological models⁵ and through measurements at 2.6 GHz.¹⁹ Interestingly, the latter work demonstrates a significantly decreased AC impedance (when compared to DC impedance) of the device (at 4 K) because of a possible capacitive coupling between the nanotube and the contact pads. In fact, in m-SWNT circuits they measure AC impedances (~ 1.7 k Ω) much lower than the quantum limited resistance for a 1-D system ($h/4e^2 \sim 6.25$ k Ω).⁴ While, this is encouraging, a further reduction in parasitics that hinder the AC performance of an electronic device can be achieved by employing a Schottky diode design in which a substrate-less membrane architecture can be employed similar to an earlier reported monolithic membrane diode (MoMED) design for a 2.5 THz receiver system.²⁰ A theoretical study conducted by Leonard et al.²¹ concluded

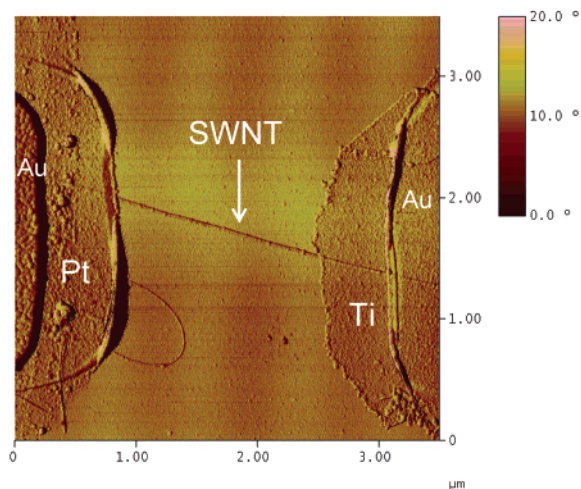
that, unlike in planar junction Schottky diodes, the Fermi level pinning in carbon nanotube Schottky diodes does not control the device properties, and as a result the threshold may be tuned for optimal device performance. They showed that for these devices the Schottky barrier height is controlled by the metal work function, unaffected by the Fermi level pinning, which offers the possibility of controlling the barrier height by the choice of the metal.

In this letter, we demonstrate Schottky diodes created by depositing two dissimilar metals at the two ends of p-type s-SWNTs, one metal with lower work function (Φ) than that of the SWNT ($\Phi_{\text{NT}} \sim 4.9$ eV) to make a Schottky contact and the other with higher Φ than that of the SWNT to make an Ohmic contact. We also show the predicted performance of these diodes as detectors at high frequencies by calculating their voltage responsivity and NEP using analytical models. The metal deposition was conducted using a self-aligned angled evaporation technique to deposit both metals with a single photoresist mask. The choice of metals used are titanium (Ti) for the Schottky contact ($\Phi_{\text{Ti}} = 4.33$ eV < Φ_{NT} ; $\Phi_{\text{NT}} \sim 4.9$ eV) and platinum (Pt) for the Ohmic contact ($\Phi_{\text{Pt}} = 5.65$ eV > Φ_{NT}). Both single s-SWNT devices and multiple s-SWNT devices have been tested. For high frequency operation, it is absolutely essential to develop these diodes with high yield of s-SWNTs per device grown in parallel, as explained later. SWNTs were grown using iron catalysts on a silicon (Si) substrate with ~ 400 nm thick thermal oxide layer. The iron nanoparticles (FeNPs) used to grow SWNTs were synthesized similarly to a previously published procedure.²² The distribution of nanoparticle diameters was 5.8 ± 2.0 nm as determined by transmission electron microscopy (TEM) using an Akisha EM-002b at 100 kV. As described previously,²³ monolayers of FeNPs were patterned onto oxidized silicon substrates using 350 nm thick PMMA (MicroChem, 950K, 4% in chlorobenzene). All the growths were done at 850 °C using methane (CH_4 –1500 sccm) and hydrogen (H_2 –50 sccm) at a pressure of 780 Torr. The resulting SWNTs were characterized by atomic force microscopy (AFM) using a DI Nanoscope III with silicon probes in tapping mode. The tube diameters were measured to be between 1 and 3 nm. TEM studies revealed that most of the nanotubes were single-walled, although we cannot rule out the possibility of occasional double walled ones.

The device fabrication involved patterning the electrodes directly over the nanotubes using three masking layers stacked as follows: 700 nm thick 950 K molecular weight poly(methyl methacrylate) (PMMA), 15-nm thick Ti and 1.4 μm thick photoresist, with PMMA being the bottom-most layer used to protect the nanotube during further processing. The photoresist was patterned to create an “isolation block” between the two ends of the nanotube followed by the removal of the Ti layer in CF_4/O_2 plasma. The isolation block facilitates selective coating of the ends of the nanotube with dissimilar metals through angled evaporation. The electrode patterns were transferred into PMMA with ~ 1 μm undercut. At this stage the portion of SWNT that lies between the electrode patterns was still covered by the PMMA protective



(a)



(b)

Figure 1. (a) Schematic representation of the SWNT-Schottky diode showing the Ti–Schottky and the Pt–Ohmic metal layers deposited through angled evaporation. (b) AFM phase plot image of a typical SWNT-Schottky diode. The s-SWNT diameter varied from 1 to 3 nm while its length varied from 1.7 μm to 2.5 μm .

layer. Finally, the Schottky (Ti) and the Ohmic (Pt) contacts were deposited by evaporating the respective metals in series at various angles- Ti at -45° , Pt at $+45^\circ$, and the last electrode layer of Au at 0° (perpendicular to the sample surface), all in one step without breaking the vacuum. The final liftoff was done by soaking the structure in acetone to realize the SWNT Schottky device. Figure 1a shows the schematic of the device after fabrication with dissimilar metal layers, and 1b shows an AFM image of a typical device. The metal layer thicknesses were Ti ~ 20 nm; Pt ~ 17 nm; and Au ~ 100 nm, and typical lengths of SWNTs between contact pads ranged from 1.7 to 2.5 μm .

The first set of devices produced mostly contained a single SWNT bridging the gap between the metal pads in each device. As each device may have either a metallic or a semiconducting tube, the diodes were identified by gating with the substrate. Figure 2 shows rectifying I – V characteristics of devices from this set with zero gate voltage. In contrast to conventional solid-state devices, we notice that the s-SWNT devices produced in the same batch on the same substrate show significant variation in their DC characteristics. This can be attributed to a combination of the nature

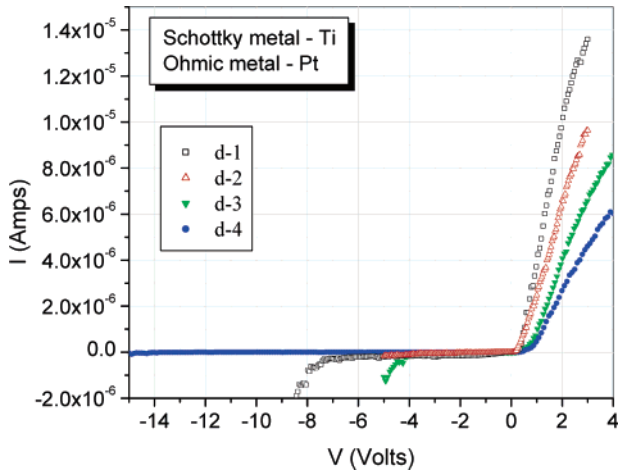


Figure 2. DC I - V characteristics of four different SWNT-Schottky devices fabricated on the same substrate in the same run (with zero gate voltage). All the devices have a single s-SWNT bridging the gap between the contact pads.

of the tubes (varying tube diameter results in varying band gaps ~ 0.3 eV to 0.6 eV, which in turn dictates the barrier height⁴), their overall lengths, and the overlapping lengths with the two metal pads (the latter two quantities contribute to the overall device impedance). The diodes exhibited high current carrying capacity, in excess of $14 \mu\text{A}$, high reverse bias breakdown voltages varying from -5 V to greater than -15 V, very small leakage currents, in the range of < 1 nA to ~ 10 nA, and high series resistances, in the range of 200 to 400 k Ω . These series resistances are, on the average, a factor of 50 larger than the lowest achievable DC resistance for a quantum-confined geometry. This large series resistance is believed to be dominated by contact resistance. Using Burke's phenomenological model,⁵ the kinetic inductance for our tubes was estimated to be ~ 10 nH ($2.5 \mu\text{m}$ long nanotube). These factors pose a significant challenge for impedance matching in high-frequency applications. Effective impedance matching requires decreasing both the individual tube impedance as well as the total device impedance. The former can be accomplished to a certain extent by annealing the contact pads,²⁴ by improved wetting properties of the deposited metal,²⁵ and by decreasing the lengths of the SWNTs (thus making it a ballistic transport device). The total device impedance can be decreased by using many nanotubes in parallel per device.

We developed a second set of devices with multiple SWNTs in parallel per device. Each device typically had 8 to 10 SWNTs, of both metallic and semiconducting nature, grown in parallel between the contact pads. The presence of m-SWNTs precludes rectification. Therefore, using a previously described procedure,²⁶ m-SWNTs were selectively burnt-out by gating off s-SWNTs by biasing the substrate to $+20$ V and increasing the total current through the device in a stepwise fashion. After every burn-out step, the I - V curves were recorded until a rectifying curve was observed. Figure 3 shows the I - V curves for one such device before and after the selective burn-out. We have successfully repeated this procedure on multiple devices.

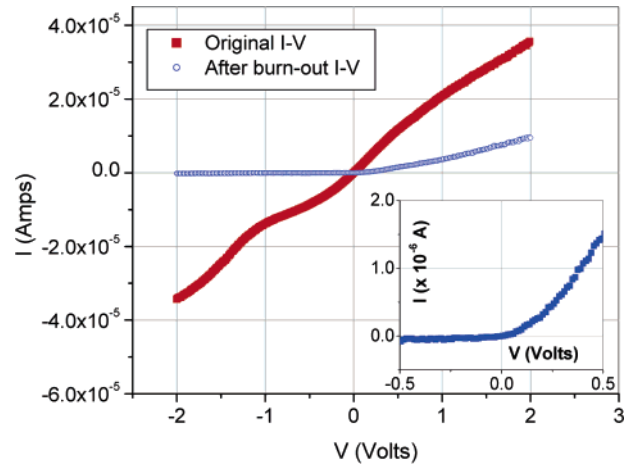


Figure 3. DC I - V characteristics of a SWNT-Schottky device with multiple SWNTs bridging the gap between the contact pads. The figure shows the change in the characteristic from resistive to rectifying upon selective burn-out of the metallic SWNTs using the procedure described by Collins et al.²⁶ The inset shows the rectified curve by itself in the low bias range.

The quality of a diode can be assessed by its ideality factor, n , calculated using the diode equation. Typically this factor lies between 1 and 2 for good diodes with $n = 1$ for an ideal diode. We have computed the value of n for the Schottky diodes presented here by fitting the curves using the following diode equation:

$$I = I_S [e^{q(V-IR_s)/nkT} - 1] \quad (1)$$

where, I = the measured total current, V = corresponding anode-cathode biasing voltage, I_S = the reverse saturation current (or the leakage current), R_s = the lumped series resistance of the device (the effective total of the contact resistances and the nanotube resistance), q = the electron charge (1.602×10^{-19} C), k = the Boltzmann constant, and T = the temperature ($^{\circ}\text{K}$). Figure 4 shows plots of the absolute value of I versus V at room temperature for diodes d1-II (with single s-SWNT) and d2-II (with multiple s-SWNTs) along with curve fits from eq 1.

In low bias ranges (as shown in the figure), the ideality curve fits well with n ranging from 1.5 to 1.9 . The important observations are the lowering of the resistance from d1-II to d2-II, and the increase in leakage current from d1-II to d2-II. In d2-II, four s-SWNTs out of nine total SWNTs survived the burn-out process. The effective R_s of 160 k Ω , post burn-out, points to the fact that the individual SWNTs still suffer from high R_s because of the contact resistance (these contacts were not annealed to avoid potential Pt delamination problems); also, the I_S increases in multiple s-SWNT devices because of the cumulative leakage effect. For the device d2-II, if we neglect the parasitic capacitances between the contact pads and the substrate (this assumption is valid if we consider a substrate-less design as in ref 20) and consider only the electrostatic capacitance of four nanotubes to the substrate (~ 81 aF per tube) and the quantum capacitance ($4C_Q \sim 970$ aF per tube), which are in series,

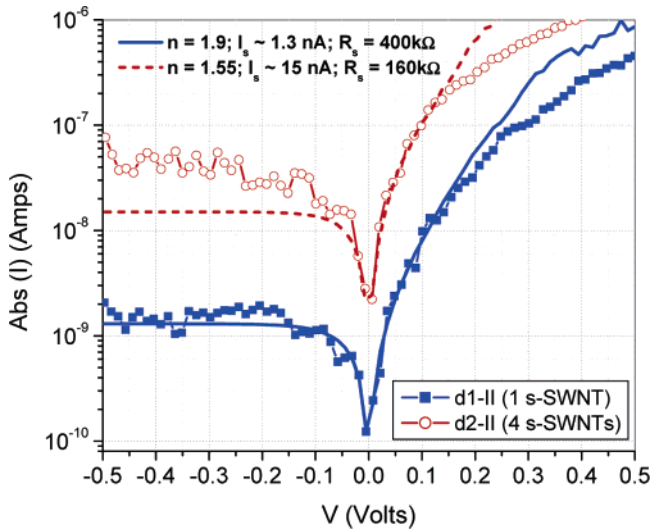


Figure 4. Ideality curve fits in low bias range for d1-II (with single s-SWNT) and d2-II (with four s-SWNTs) Schottky diodes. The curve shows the absolute magnitude of the current plotted against the corresponding voltage. The diode fits give $n = 1.5$ to 1.9 and $I_s = 1.3$ nA to 15 nA for the two diodes.

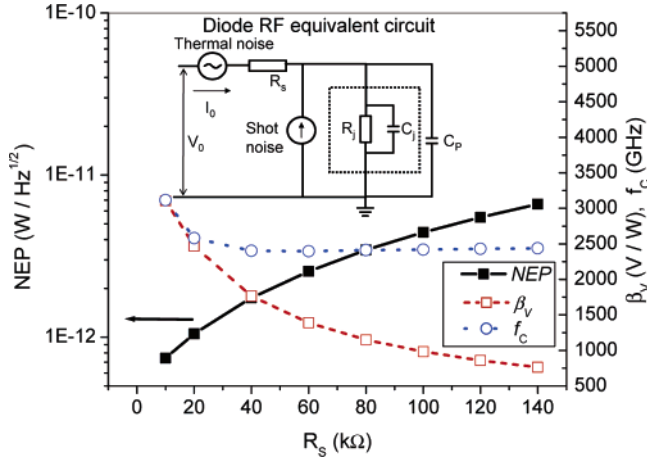


Figure 5. The dependence of the voltage responsivity (β_V), the noise equivalent power (NEP), and the cutoff frequency (f_c) on the series resistance of a hypothetical 100-nanotube SWNT-Schottky diode. The values are calculated for direct detection at 2.5 THz frequency signal at room temperature. The inset shows the diode RF equivalent circuit used in this model.

then we get an effective capacitance of $C_p \sim 75$ aF per tube (for a 2-nm diameter SWNT, 2.5- μ m long).⁵

Using the R_s and the C_p parameters, the performance prediction of d2-II SWNT-Schottky diode as a direct detector at high-frequency ranges during low bias operation has been done. This analysis uses a simplistic noise equivalent circuit²⁷ as shown in the inset of Figure 5. In this analysis we also neglect the role of the inductance (L) of the system because of the high value of R_s and because we assume that L can be tuned out using external circuit elements. We have estimated three important performance parameters, which are, the cutoff frequency (f_c), the voltage responsivity (β_V), and the noise equivalent power (NEP). The cutoff frequency, f_c , gives the upper frequency limit of a device for an AC response, which directly relates to the device-associated delay

times. β_V is defined as the detector signal strength generated per unit input power of the AC signal (V/W) and the NEP is defined as input power required to bring the signal-to-noise ratio to unity in a unit video bandwidth ($W/\sqrt{\text{Hz}}$). For high-frequency operation it is desirable to have high f_c , high β_V , and low NEP from a diode. In the performance analysis presented here, the responsivity and the NEP of the SWNT-Schottky diodes have been estimated for 2.5 THz frequency, which is a region of interest for space-borne applications (for example, the remote detection of oxygen and hydroxyl (OH) species whose characteristic emission lines are present at this frequency), using relations shown below. A detailed discussion of these relations is beyond the scope of this letter and can be found in earlier publications.^{27–30} These relations are based upon the circuit shown in the inset of Figure 5, in which, R_j and C_j refer to the diode's dynamic junction resistance and capacitance, respectively. In the model used here it is important to note that in low bias ranges, which is the concerned operating region of the diode, R_j and C_p have the dominant influence on f_c (the effect of C_j is negligibly small because of the nanotube area). The cutoff frequency is calculated as

$$f_c = \frac{1}{2\pi R_j C_p} \sqrt{\frac{R_s + R_j}{R_s}} \quad (2)$$

where

$$R_j = \frac{nkT}{q(I_0 + I_s)} \quad (3)$$

In eq 2 the quantity under the square root tends to unity for $R_s \gg R_j$ (which is true as long as R_s is in the range of hundreds of k Ω). In eq 3 above, I_0 is the DC bias current (same as I in eq 1) corresponding to the optimized DC bias voltage, V_0 . V_0 is calculated iteratively to achieve the least noise power for a given diode and a given detection frequency. V_0 , in turn, depends on R_s . The voltage responsivity, β_V , is calculated as

$$\beta_V = \gamma_0 \beta R_{VT} (V/W) \quad (4)$$

where, $\gamma_0 = R_j / \{(R_s + R_j)[1 + (f/f_c)^2]\}$, $\beta = q/2nkT$, and $R_{VT} = R_s + R_j$, assuming an infinite load and an antenna matched source to the diode. The NEP is calculated by dividing the voltage noise density, v_n ,²⁹ by the voltage responsivity, β_V .

$$\text{NEP} = \frac{v_n}{\beta_V} (W/\sqrt{\text{Hz}}) \quad (5)$$

where

$$v_n = \sqrt{4kT_D R_{VT}} (V/\sqrt{\text{Hz}})$$

where T_D is the diode equivalent noise temperature.²⁹ As R_s decreases, β_V increases at a higher rate than the rate of decrease of v_n , thus effectively decreasing the NEP.

We have calculated the above-mentioned performance parameters for the device d2-II described before using the following values: $R_s = 640$ k Ω /tube (for four tubes in parallel the effective R_s is 160 k Ω ; in comparison, R_j is only ~ 796 Ω /tube), $C_P = 75$ aF, $n = 1.55$, $I_S = 15$ nA. For this device, we find that the optimized bias voltage, V_0 , is equal to 0.20 V, which is in a region where the ideality curve fit begins to deviate (see Figure 4). For a realistic estimate, we use an operating bias of $V_0 = 0.17$ V, which is the maximum bias voltage where the curve fit still holds within reason. Therefore, for an operating bias voltage, $V_0 = 0.17$ V, β_V (d2-II) ~ 2.6 V/W; NEP_(d2-II) $\sim 2.0 \times 10^{-8}$ W/ $\sqrt{\text{Hz}}$; and $f_{C(d2-II)}$ ~ 0.54 THz. For comparison we have calculated the same parameters for a GaAs solid-state Schottky diode (model 1T15) developed by Crowe et al.³¹ using the following values: $R_s = 20$ Ω , $C_P = 250$ aF, $n = 1.3$, $I_S = 10$ fA, and we get for $V_0 = 0.59$ V (optimized for the SWNT-Schottky device), $\beta_{V(\text{GaAs})} \sim 4116$ V/W; NEP_(GaAs) $\sim 5.4 \times 10^{-13}$ W/ $\sqrt{\text{Hz}}$; and $f_{C(\text{GaAs})} \sim 7$ THz. These results indicate that the predicted high frequency performance of d2-II is quite poor compared to that of the state-of-the-art. This poor performance is caused predominantly by the high value of R_s , which indirectly decreases f_C , and directly brings down β_V and the NEP (this is easy to see as resistance is a source of thermal noise). In addition to this degradation in device performance at high frequencies, the high series resistance also introduces nontrivial concerns for impedance matching. To complete this argument, if we are able to change the SWNT Schottky diode such that it contains at least 100 tubes of 2-nm diameter and 100-nm length in parallel, each tube with $R_s = 10$ k Ω , $C_P = 3$ aF, $n = 1.3$ (similar to the GaAs device), $I_S = 1$ nA, then we get for $V_0 = 0.17$ V, $\beta_V \sim 3105$ V/W; NEP $\sim 7.4 \times 10^{-13}$ W/ $\sqrt{\text{Hz}}$; and $f_C \sim 3.1$ THz. This device enjoys much higher voltage responsivity and NEP (compared to those of d2-II) that are in a comparable range to those of the GaAs device (the cutoff frequency is lower because of the lower optimized biasing voltage). Except for the R_s , which is approaching the quantum limit (6.25 k Ω), all other assumed parameters are reasonably practical as explained ahead. The hypothetical device has a significantly decreased C_P because of the assumed tube length that is shorter by a factor of 25 compared to that in d2-II. This results in a smaller electrostatic capacitance (~ 3.24 aF) and hence a smaller overall capacitance (the in-series quantum capacitance is ~ 38.8 aF, still too large to affect the overall C_P). The assumed value of n is also within reason as the device d2-II, which is much inferior compared to the hypothetical device, already has n of 1.55, and by decreasing R_s per tube (see eq 1) of the device, the effective n is expected to improve at least partially. For the same hypothetical SWNT Schottky diode, Figure 5 shows the trend of f_C , β_V , and the NEP variation with respect to R_s (all calculations are performed at room temperature with V_0 optimized for the lowest NEP at 2.5 THz).

For high-frequency technological applications of carbon nanotubes, our results suggest how key impedances should be adjusted to improve device performance. It has been observed by Burke et al.¹⁹ that the AC resistance in the SWNT device could become considerably lower because of the capacitive coupling between the nanotube and the contact pads. In this case, it is indeed possible to bring R_s down to the order of a few k Ω , which then should improve the NEP better than that of its solid-state counterpart. Also, by growing hundreds of nanotubes in parallel per device, the effective impedance (series resistance and the kinetic inductance) can be decreased to achieve proper impedance matching. To decrease parasitic capacitances that have been neglected in this analysis, one can employ the substrate-less dielectric membrane design²⁰ in which the substrate is relegated to just a frame to support the dielectric membrane upon which the device is fabricated. This, especially, is an attractive option for high frequency applications that cannot be readily achieved in an FET design in which a gate is a necessity either in the substrate form (bottom gate) or as a top gate. In essence, the SWNT Schottky diodes with multiple parallel tubes per device with individually reduced resistances to the order of a few k Ω promise superior performance compared to that of the state-of-the-art solid-state Schottky diodes for applications at high frequencies. Along with the device development itself, significant developmental work is still required to achieve impedance matching and input power coupling at submillimeter wave frequencies.

Acknowledgment. During the preparation of this manuscript we became aware of a similar work by Jie Liu et al of Duke University presented at the American Physical Society's March 2005 meeting at Los Angeles, CA that was held from March 21–25, 2005. This research was carried out at the Jet Propulsion Laboratory (JPL), California Institute of Technology, under a contract with National Aeronautics and Space Administration (NASA). This work was supported by JPL's Research and Technology Development (R&TD) Fund. Authors, H.M.M. in particular, extend special thanks to Dr. Goutam Chattopadhyay for very valuable discussions concerning diode direct detectors and we also thank Dr. Anders Skalare, and Mr. Edward Luong of JPL's Submillimeter Wave Advanced Technology (SWAT) Group for useful discussions and for the device fabrication support.

References

- (1) Siegel, P. H. *IEEE Trans. Microwave Theory Technol.* **2002**, *50*, 910–928.
- (2) Ijima, S. *Nature* **1991**, *354*, 56–58.
- (3) Durkop, T.; Getty, S. A.; Cobas, E.; Fuhrer, M. S. *Nano Lett.* **2004**, *4*, 35–39.
- (4) Dresselhaus, M. S.; Dresselhaus, G.; Avouris, Ph., Eds.; *Carbon Nanotubes*; Springer: Berlin, 2001; Vol. 80.
- (5) Burke, P. J. *Solid-State Electron.* **2004**, *48*, 1981–1986.
- (6) Mintmire, J. W.; Dunlap, B. I.; White, C. T. *Phys. Rev. Lett.* **1992**, *68*, 631–634.
- (7) Hamada, N.; Sawada, S.; Oshiyama, A. *Phys. Rev. Lett.* **1992**, *68*, 1579–1581.
- (8) Saito, R.; Fujita, M.; Dresselhaus, G.; Dresselhaus, M. S. *Appl. Phys. Lett.* **1992**, *60*, 2204–2206.
- (9) Wildoer, J. W. G.; Venema, L. C.; Rinzler, A. G.; Smalley, R. E.; Dekker, C. *Nature* **1998**, *391*, 59–62.

- (10) Odom, T. W.; Huang, J.; Kim, R.; Lieber, C. M. *Nature* **1998**, *391*, 62–64.
- (11) Tans, S.; Verschueren, A.; Dekker, C. *Nature* **1998**, *393*, 49–52.
- (12) Martel, R.; Schmidt, T.; Shea, H. R.; Hertel, T.; Avouris, P. *Appl. Phys. Lett.* **1998**, *73*, 2447–2449.
- (13) Zhou, C.; Kong, J.; Dai, H. *Appl. Phys. Lett.* **1999**, *76*, 1597–1599.
- (14) Kong, J.; Franklin, N. R.; Zhou, C.; Chapline, M. G.; Peng, S.; Cho, K.; Dai, H. *Science* **2000**, *287*, 622–625.
- (15) Collins, P. G.; Bradley, K.; Ishigami, M.; Zettl, A. *Science* **2000**, *287*, 1801–1804.
- (16) Avouris, P.; Appenzeller, J.; Martel, R.; Wind, S. J. *Proc. IEEE*, **2003**, *91*, 1772–1784.
- (17) Lee, J. U.; Gipp, P. P.; Heller, C. M. *Appl. Phys. Lett.* **2004**, *85*, 145–147.
- (18) Fuhrer, M. S.; Nygard, J.; Shih, L.; Forero, M.; Yoon, Y-G.; Mazzone, M. S. C.; Choi, H. J.; Ihm, J.; Louie, S. G.; Zettl, A.; McEuen, P. L. *Science* **2000**, *288*, 494–497.
- (19) Li, S.; Yu, Z.; Yen, S.-F.; Tang, W. C.; Burke, P. J. *Nano Lett.* **2004**, *4*, 753–756.
- (20) Gaidis, M. C.; Pickett, H. M.; Smith, C. D.; Smith, R. P.; Martin, S. C.; Siegel, P. H. *IEEE Trans. Microwave Theory Technol.* **2000**, *48*, 733–739.
- (21) Leonard, F.; Tersoff, J. *Phys. Rev. Lett.* **2000**, *84*, 4693–4696.
- (22) Hyeon, T.; Lee, S. S.; Park, J.; Chung, Y.; Na, H. B. *J. Am. Chem. Soc.* **2001**, *123*, 12798–12801.
- (23) Wong, E. W.; Bronikowski, M. J.; Hoenk, M. E.; Kowalczyk, R. S.; Hunt, B. D. *Chem. Mater.* **2005**, *17*, 237–241.
- (24) Zhang, Y.; Ichihashi, T.; Landree, E.; Nihey, F.; Ijima, S. *Science*, **1999**, *285*, 1719–1722.
- (25) Javey, A.; Guo, J.; Wang, Q.; Lundstrom, M.; Dai, H. J. *Nature* **2003**, *424*, 654–657.
- (26) Collins, P. G.; Arnold, M. S.; Avouris, P. *Science*, **2001**, *292*, 706–709.
- (27) Cowley, A. M.; Sorenson, H. O. *IEEE Trans. Microwave Theory Technol.* **1966**, *14*, 588–602.
- (28) Dicke, R. H. *Rev. Sci. Instrum.* **1946**, *17*, 268–275.
- (29) van der Ziel, A. *Noise in Solid State Devices and Circuits*; Wiley: New York, 1986; App. A3.
- (30) Shousha, A. H. M. *J. Phys. D: Appl. Phys.* **1982**, *15*, 669–675.
- (31) Crowe, T. W.; Mattauch, R. J.; Roser, H. P.; Bishop, W. L.; Peatman, W. C. B.; Liu, X. *IEEE Proc.* **1992**, *80*, 1827–1841.

NL050829H